Location of the Active Sites for Ethylcyclohexane Hydroisomerization by Ring Contraction and Expansion in the EUO Zeolitic Framework

Ester Gutierrez-Acebo, Jerôme Rey, Christophe Bouchy, Yves Schuurman, Céline Chizallet

Location of the Active Sites for Ethylcyclohexane Hydroisomerization by Ring Contraction and Expansion in the EUO Zeolitic Framework

Ester Gutierrez-Acebo,[1] *Jérôme Rey,*[1] *Christophe Bouchy,*[1] *Yves Schuurman,*[2] *Céline Chizallet*[1,]*

[1]IFP Energies nouvelles, Rond-point de l'échangeur de Solaize, BP 3, Solaize, 69360, France

[2]Université Lyon 1, CNRS, UMR 5256, IRCELYON, Institut de recherches sur la catalyse et l'environnement de Lyon, 2 avenue Albert Einstein, F-69626 Villeurbanne, France

Corresponding author: celine.chizallet@ifpen.fr

ABSTRACT. Identifying the location of the active sites in a zeolite is a current challenge, impeding the design of optimal catalysts. In this work, we identify the location of the most active sites of 1-ethylcyclohexene isomerization in the EUO framework (10 MR channels, 12 MR side pockets), thanks to DFT calculations corroborated by experiments. Skeletal isomerization of cycloalkenes is a crucial industrial reaction for the bifunctional isomerization of ethylbenzene. Ethylcyclohexene is protonated by framework protons into cyclic carbenium ions, which undergo ring contraction-expansion reactions through protonated cyclopropane (PCP) like transition states. *Ab initio* calculations clearly show that the acid sites located at the intersection between the channel and the pocket stabilize much less the cyclic carbenium ions involved in the reaction than 12 MR pockets and 10 MR channel sites, due to stronger dispersion stabilizing interactions. This computational finding is fully confirmed experimentally by the comparison of the catalytic performances of the H-EU-1 and H-ZSM-50 zeolites in ethylcyclohexane hydroisomerization. Both zeolites possess the EUO structure, but with different location of the acid sites. The ratio in turnover frequencies is quantitatively rendered by the DFT calculated free energy profiles. Diffusion measurements reveal similar ethylcyclohexane diffusion times for the two zeolites, supporting that the difference in activity is primarily driven by the location of the active sites.

Keywords: zeolite, naphtene, Protonated CycloPropane, confinement effect, side pocket, channel, EU-1, ZSM-50.

1. INTRODUCTION

Zeolites are very powerful aluminosilicate catalysts for a variety of reactions in refining, petrochemistry,[1] pollution abatement,[2] and also promising candidates for biomass conversion.[3-4] Their crystalline nature and the large variety of structures makes possible the design of catalysts from structural considerations.[5-7] For acid catalyzed reactions, such as isomerization and cracking, the active sites are protons related to the aluminum atoms. A main challenge however consists in the identification of the precise location of the active sites of a given zeolite, as the local topology may strongly differ from one T site to another.[8] This is first of all due to the limited number of zeolites with more or less known location of aluminum atoms.[5,9-17] Then, even once the location is known, it is generally not unique so that identifying the precise location of the most stable intermediates and transition states is not straightforward. This is however a condition for the design of better catalysts. The case of the EUO framework is illustrative in that respect. This structure is composed of a monodimensional channel pore system (10 MR) with side pockets (12 MR). Two zeolites exhibiting this structure type, EU-1 and ZSM-50, were deeply investigated in particular by neutron diffraction.[18-19] In the case of ZSM-50, the aluminum atoms are located mainly in the intersection between the channel and the pocket whereas in the case of the EU-1,[18-19] they are found either inside the pocket or in the channels. In contrast with EU-1, the synthesis of ZSM-50 at low Si/Al ratio is challenging.[20]

Naphthenes (cycloalkanes) are an important part of the feedstock converted in refineries and therefore, a matter of interest for the petroleum industry. Nevertheless, their reactivity has not been deeply studied contrary to the case of paraffins. Naphthenes have a more complex reactivity than linear paraffins. This fact is due to the possibility of forming tertiary carbons by adding additional alkyl groups, and to the higher number of possible conversion pathways (including

dehydrogenation into cycloalkenes, then isomerization, ring opening and cracking).[21] Typically, the most abundant naphthenic components in the hydrocarbons produced from petroleum are 5- and 6- carbon rings,[21] due to minimum tension in the ring compared to the 3 and 4 carbons rings. In petrochemistry, ethylbenzene hydroisomerization is of importance in the paraxylene production. Paraxylene is a highly sought-after product used in the manufacture of the terephtalic acid, employed for nylon production. Traditionally, the ethylbenzene hydroisomerization employs a bifunctional catalyst[22] composed by a metal compound (responsible of the hydro/dehydrogenation function, HD/DHD) dispersed over an acidic support (isomerization and cracking function). The EU-1 zeolite is industrially used as acidic function for ethylbenzene hydroisomerization.[1] The location of the active sites is an important question for this zeolite family, as the confinement effect is expected to differ significantly between the 10 MR channel, the 12 MR side-pockets and the intersection between the channels and the pockets.

Ethylbenzene hydroisomerization over bifunctional catalysts involves the isomerization of ethylcylcohexenes over the Brønsted acid phase (the zeolite).[23] Reactions involving these cycloalkenes are expected to implicate carbocations. These cyclic carbenium ions can be isomerized by hydride shift, methyl shift and ring contraction expansion *via* protonated cyclopropane (PCP) steps.[23-29] The alkylnaphthenes rearrangements have been classified by Weitkamp[26] in two main categories: type A and type B isomerizations. In type A isomerization, the branching degree remains constant whereas in type B isomerization the branching degree is modified. Type A isomerization is considered to be faster than type B isomerization.[21,26,30-32] Molecular insight is strongly lacking for these reactions, regarding not only the relevant mechanisms if not as well, the intermediate / transition states involved and the quantification of their stability.

In the present work, we propose a Density Functional Theory (DFT) approach to determine these features in the EUO framework. We also aim at identifying the location of the most active sites for these reactions with the same approach, complemented with experimental comparison of the catalytic performances of the H-EU-1 and H-ZSM-50 zeolites. Furthermore, some diffusion measurements have been performed in order to evaluate the possible influence of the diffusion in the catalytic performance.

The chosen reaction is the isomerization of ethylcyclohexene ($ECH^{=}$, obtained from the dehydrogenation of ethylcyclohexane (ECH), or the hydrogenation of ethylbenzene) into other branched substituted cycloalkenes. We showed experimentally[33] that a relevant apparent reaction pathway consists in the transformation of ECH^{+} (ethyl-cyclohexenium) into $EMCP^{+}$ (ethylmethyl-cyclopentenium), then into $DMCH^{+}$ (dimethyl-cylclohexenium) and finally into $TMCP^{+}$ (trimethyl-cyclopentenium). Experimentally, many products are obtained (16 re-hydrogenated products, meaning an even higher number of alkene structures), belonging to the three EMCP, DMCH, TMCP families. It prevents the exhaustive computational investigation of the formation of all of them on all the sites of the zeolite. Thus, we decided to make a relevant choice so as to represent the three families of products. The reaction sequence selected here (Figure 1) takes into account members of each of the three families, focusing on tertiary carbenium ions, which are expected to be stable species.

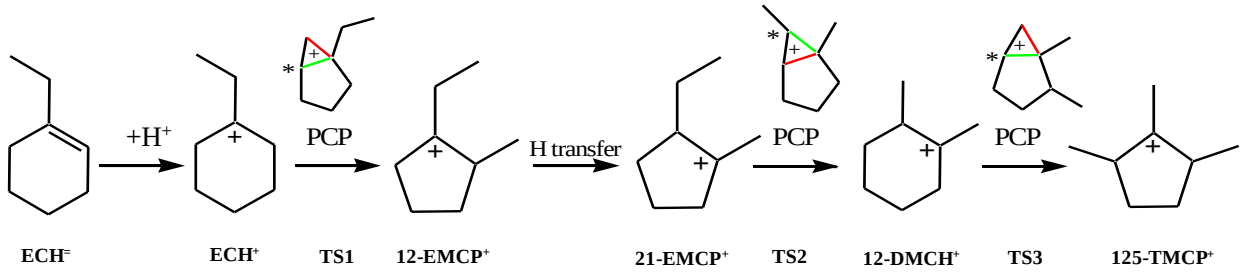

Figure 1. One ethylcyclohexene isomerization reaction pathway, passing through tertiary carbocations. * Hydrogen shifting. The bond to be broken (in the forward direction) is depicted in red and the forming bond in green.

For non-cyclic species it is not always clear from experiments whether carbenium ions exists as free or adsorbed species inside the zeolite pores, or if they are covalently bonded to framework oxygen forming alkoxide intermediates (Figure 2). This depends on the zeolite but also on the nature of the olefin and the carbenium (substitution, delocalized nature).[34] From catalytic hydrocraking experiments, carbenium appear as most probable intermediates.[35-36]

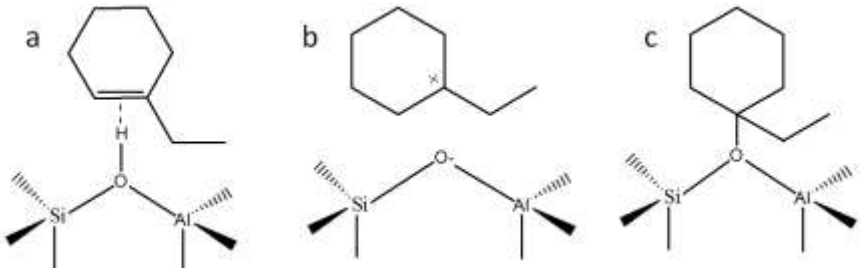

Figure 2. Three possible forms for adsorbed 1-ethylcyclohexene at the bridging acid site of a zeolite: a) π-complex; b) carbenium, c) alkoxide.

Earliest *ab initio* calculations used small clusters. These calculations indicated that adsorbed carbenium and carbonium ions (active intermediates of acid-catalyzed transformations of small hydrocarbons up to C_4) on zeolites were not reaction intermediates. Indeed, they were the transition states of the alkene protonation elementary step, whose products were their corresponding alkoxides, avoiding charge separation.[37-38] The same conclusion was obtained for PCP species,[39] isolated as transition states only.

However, the steric constraints and electrostatic field provided by the zeolite framework play an important role which cannot be taken into account by very small clusters as the one used in the earliest studies. These factors are better taken into account by periodic approaches or by big

clusters simulations. Both factors can affect not only the stability of alkoxides, which is very sensitive to the local site geometry,[40-41] but also the stability of carbenium ions, sensitive to the electrostatic field intensity.[42-44] Depending on the level of theory (DFT-GGA *versus* DFT-GGA plus dispersion corrections *versus* hybrid functionals) and on the location of the Brønsted acid site (itself function of the considered zeolite framework), the carbenium species can however still be considered as transition states for the protonation of alkenes to alkoxides,[41-42] or as local energy minima, thus reaction intermediates.[41,43] Periodic studies of the isomerization through PCP species are very scarce. Demuth et al.[45] focused on the isomerisation 2-pentene in H-ZSM-22. Huang et al. recently reported about hex-3-ene isomerization in H-ZSM-5.[46] The PCP was found as a transition structure, alkoxides being the reaction intermediates in both studies.

Higher level calculations, such as the hybrid MP2 calculations performed by Tuma et al.[47] revealed the tert-butyl carbenium ion as a reaction intermediate, which was not the case at the PBE level. Nonetheless, it was less stable as compared to the π complex and alkoxides. The consideration of thermal effects were also shown to affect the conclusions about the stability of carbenium ions as intermediates. Tuma and Sauer[48] took into account the influence of the temperature in the stability of the reaction intermediates and transition states, starting from periodic static DFT - PBE calculations. The carbenium appeared as the most stable species with respect to alkoxides when the temperature was raised over 120 K. More recently, studies from van Speybroeck et al.[49-50] compared static and molecular dynamic methods for measuring the stability of adsorbed butene and pentene in H-ZSM-5. By *ab initio* molecular dynamics (AIMD) at 323 K, linear alkoxides, alkene π complex and tertiary carbenium ions were found as the favored intermediates. Nonetheless, at 773 K, secondary and tertiary alkoxides were not stable, contrary to the carbenium ion, which was found as a stable intermediate.

To sum up, in spite of all the performed studies, the answer to the question if carbenium ions are reaction intermediates or transition states remains elusive. Very scarce are the studies devoted to reactions proceeding via PCP species. Moreover, whereas many work has been done about olefins chemisorption on acidic zeolites,[40-43,45,47-51] the reactivity of naphthenes was only very barely investigated by DFT. Some cyclic cations have been experimentally observed to be important long-lived intermediates in some reactions of hydrocarbons on zeolites.[52] A DFT study of the cyclohexene interaction in H-ZSM-5[53] revealed the formation of carbenium species instead of alkoxides as local energy minima. The bulkiness of cyclic carbenium with respect to non-cyclic ones may indeed be a factor of easier stabilization of cyclic carbenium, preventing the approach to framework oxygen atoms.

Concerning the mechanism of ring contraction and expansion of cyclic olefins, over the acid sites, no DFT work has been published to date, to the best of our knowledge. Ring contraction-expansion reactions are also of interest in the Methanol to Olefin context, and were studied by computational approaches,[54-58] but the nature of the reaction intermediates and transition state differs as in MTO the starting points are protonated aromatics, whereas we start here from protonated cycloalkenes. As mentioned previously, the first periodic study of isomerization reactions through PCP concerned a non-cyclic short molecule, namely 2-pentene, in H-ZSM-22, at the GGA (PW91) level, by Demuth et al.[45] Note that the reactants and products were found in the form of alkoxides, and not carbenium ions, which may have had an influence on the reaction profile. The lower-activated (about 100 $kJ.mol^{-1}$) mechanism proposal involved up to three different transition states (among which an edge-protonated PCP) and two intermediates (a secondary carbenium ion and a neutral dimethylcyclopropane DMCP).

Therefore, the objective of this study is to investigate the reactivity of the cycle contraction-expansion in the context of the ethylcyclohexene isomerization (itself obtained from the dehydrogenation of ethylcyclohexane), identifying the location of the most active sites of an EUO type zeolite for this reaction. To do so, first the stability of the different forms of the adsorbed reactant (carbenium, alkoxide and π-complex) have been evaluated, as well as the intermediates and transition states for the mechanism shown in Figure 1. An exhaustive screening of all the possible active sites of an EUO type zeolite has been as well performed (Figure 3). Furthermore, an experimental evaluation of the activity of zeolites H-EU-1 and H-ZSM-50 has been carried out for the ethylcyclohexane hydroconversion, so as to challenge the calculated features in terms of location of the most active sites. To complete this evaluation, Temporal Analysis of Products (TAP) experiments[59] of ethylcyclohexane diffusion in both zeolites H-EU-1 and H-ZSM-50 has been performed, to check if diffusional issues can impact the catalytic activity of these two zeolites.

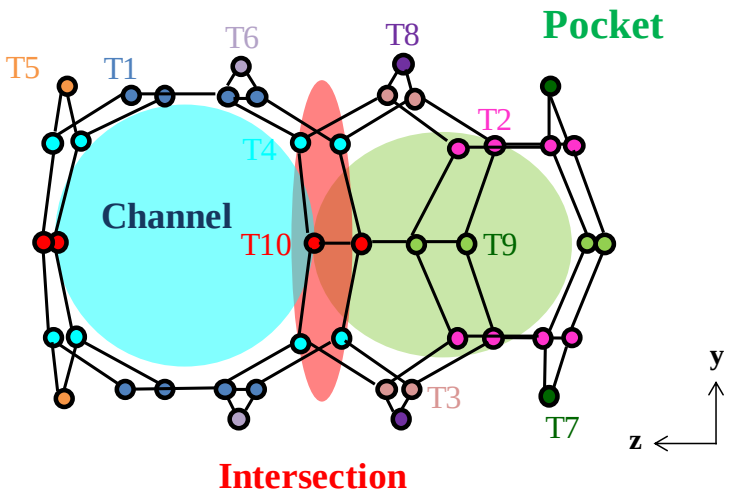

Figure 3. Section of the EUO framework structure showing the different active sites analyzed in this study: pocket – green zone (light green T9, dark pink T2, light pink T3, dark green T7, and dark purple T8), channel –blue zone (dark blue T1, orange T5, and light purple T6) and intersection between the pocket and the channel – red zone (red T10 and light blue T4) [1 0 0]. Adapted with permission from ref. [19]. The oxygen atoms are not included and the silicon atoms are represented as colored circles.

2. EXPERIMENTS AND METHODS

2.1 DFT calculations

Periodic DFT calculations were performed with the PBE (Perdew, Burke and Ernzerhof) exchange-correlation[60] as implemented in VASP 5.3.[61-62] The projected augmented wave (PAW) method[63] was used to describe the core-electron interactions, and the plane wave basis set was limited to a kinetic cutoff energy of 400 eV except for the optimization of the cell dimensions, for which the cutoff was set at 800 eV. Van der Waals corrections as proposed within the D2 Grimme formalism[64] were applied. The convergence criterion for the electronic self-consistent field relaxation was fixed to 10^{-7} eV. All calculations were performed at the gamma point.

The bulk cell parameters and ionic positions of EU-1 and ZSM-50 (EUO type) were obtained from International Zeolite Association (IZA) database[65] and then reoptimized in the purely siliceous form with an increased energy cutoff of 800 eV (initial parameters from IZA: a = 13.3778 Å, b = 13.3778 Å, c = 20.5820 Å, α=β= 90°, γ=62.6° , parameters after optimization: a = 13.2189 Å, b = 13.3266 Å, c = 20.3045 Å, α=90.0°, β= 89.9°, γ=62.8°). The amount of aluminum atoms (together with a proton per Al) in the zeolite framework came from a Si/Al equal to 15, commonly considered experimentally,[33,66-67] and representative of the EU-1 used in the present study. Since the primitive EUO structure cell possesses 112 T sites, the number of aluminum atoms needs to be between 3 and 4. As a matter of simplicity it has been chosen 3. In the beginning of the study two different cells with three different locations of the Al on each were investigated. The sites choice was basically done taking into account the most different locations in the structure: the pocket, the channel, and their intersection. The sites are named from the number (IZA) of the T atom substituted by Al, and the number of the oxygen atom holding the proton. The first cell contains exchanged T10O12, T1O1, and T9O6 sites, whereas

the second one contains exchanged T4O12, T1O2 and T9O20 sites. Afterwards, in order to test the other active T sites all the silicon atoms were successively substituted by Al, the proton being put in an accessible position. The relative stability of the alumination configurations considered (Table S1) ranges over 44 $kJ.mol^{-1}$, consistently with previous observations made on other frameworks.[44 ,68-69] Full geometry optimizations (zeolite plus hydrocarbons) of the reaction intermediates were performed using a conjugate gradient algorithm, with a convergence criterion on forces of 0.005 $eV.Å^{-1}$.

The Nudged Elastic Band (NEB) method[70] was used to locate the transition states. The number of images to investigate reaction pathways between the reactant and the product is 8. To start with, an interpolation scheme involving both Cartesian and internal coordinates was used (Opt'n-Path developed by Paul Fleurat-Lessard).[71] We basically perform 50 NEB steps before optimizing the structure of the highest energy image. The optimization consists in a quasi-Newton calculation,[72] sometimes followed by a Dimer calculation[73-74] if the quasi-Newton had difficulties to converge.

Harmonic frequency calculations were performed on optimized structures (all atoms of the cell moving) with a displacement of $\pm$0.02 Å around the equilibrium atomic positions. The objective of these calculations was double: i) to identify the true local energy minimum / saddle point nature of the optimized intermediates and transition structure, ii) to deduce vibrational free energies.

To achieve objective i), most of the time some refinements of the intermediate and transition structures had to be performed, to get zero (in the case of intermediates) or only one (in the case transition structures) imaginary frequencies, which was scarcely the case right after the Dimer or quasi-Newton optimizations, despite stringent convergence criteria. Line minimization methods

were applied, thanks to algorithms developed by Tomáš Bučko (Univ. Bratislava).[75] The procedure was repeated until the configuration with a correct vibrational spectrum was identified (typically 1 to 6 repeated cycles are needed). An example of such a sequence is given in Supporting Information S1.

For each transition structure, the connection with the expected reactants and products was established thanks to the intrinsic reaction coordinate (IRC) approach. This concept has been introduced by Fukui[76-77] and was successfully applied within VASP in the case of hydrocarbon reactions in zeolites.[75] The IRC is the steepest descent path, starting from the transition state in the direction of the transition vector (corresponding to the imaginary vibrational frequency determined *via* vibrational analysis). Examples are given in Supporting Information S2. The algorithm stops if the energy increases over 20 successive steps. Structures identified at the end of the IRC were re-optimized with a convergence criterion on forces of 0.005 $eV.Å^{-1}$.

The adsorption energy E_{ads} of all the considered species was calculated, using isolated ethylcyclohexene and the empty zeolite as references. For each of these species, the Gibbs free energy was then calculated according to the equations given in Supporting Information S3 by considering the rotational, translational, and vibrational degrees of freedom for gas-phase ethyl-cyclohexene and the vibrational degrees of freedom only for the zeolite models. The translational (and rotational) degrees of freedom were again decoupled from the vibrational one before estimating vibration partition functions.

2.2 Catalysts preparation

Commercial zeolite EU-1 supplied by Zeolyst was obtained in the protonic form according to the procedure described in reference 33. ZSM-50 was synthesized according to the protocol

given in reference 19. ZSM-50 was obtained in the protonic form as follows. The zeolite was first calcined in order to remove the dibenzyldimethylammonium organic template. The calcination was done under an air flow (2 NL $h^{-1}g^{-1}$) at 150°C (1h), 250°C (1h), 550°C (1h), 650°C (1h), 750°C (1h) and finally at 800°C for 10 h. The zeolite was then exchanged with an ammonium nitrate solution and calcined with the same protocol used for EU-1.[33]

The H-EU-1 and H-ZSM-50 bifunctional catalysts were obtained by mixing 20% wt. of the corresponding zeolite with 80% wt. of alumina loaded with 1% wt. platinum. The experimental protocol is described elsewhere.[19,33] The mechanical mixtures were pelletized with a hydraulic press, crushed, and sieved to obtain a pellet size between 350 and 500 µm before catalytic tests. Main features of the two bifunctional catalyst are provided Table 1 .

Table 1: Bifunctional catalysts used in this study.

Metallic function	Acidic function	Catalyst composition	Catalyst name	n_{Pt*} (µmol/g)	n_{A**} (µmol/g)	n_{Pt}/n_A
1.05%wt Pt-Al_2O_3	H-EU-1	80%wt Pt-Al_2O_3 / 20%wt H-EU-1	1%Pt-Al_2O_3 /H-EU1	43	147	0.29
1.05%wt Pt-Al_2O_3	H-ZSM-50	80%wt Pt-Al_2O_3 / 20%wt H-ZSM-50	1%Pt-Al_2O_3 /H-ZSM50	43	106	0.42

* micromoles of platinum surface sites per gram of catalyst, ** micromoles of Brønsted acid sites per gram of catalyst

2.3 Material characterizations

Zeolites were characterized by X-ray fluorescence to determine the global Si/Al molar ratio. XRF analyses were performed with a Thermo scientific ARL Perform'X. ^{27}Al magic angle

spinning nuclear magnetic resonance (MAS NMR) was employed to determine the percentage of framework and extra-framework aluminum. NMR experiments were performed using a Bruker Ultrashield 400 MHz spectrometer equipped with a 4 mm CP MAS probe head at room temperature. The MAS rate was 12 kHz for all experiments, the sequence used for Al was a zg sequence and a delay time of 0.5 s. The number of Brønsted acid sites was calculated from these two techniques (number of Al^{IV} considered to be equal to the number of Brønsted sites). For this calculation, Na residual presence, measured by atomic absorption spectroscopy (AAS) has been also considered. Crystallinity was measured by X-ray diffraction (XRD) using a X'Pert Pro diffractometer from Philips Analytical, using a Cu Kα radiation (λ = 1.5406 Å). Diffraction profiles were scanned using the step mode over a 2θ range of 5–40°, in steps of 0.02° for six hours with a step time of 5 s at each point. Nitrogen adsorption measurements were carried out at -200°C on an automatic Micromeritics ASAP 2420 apparatus. Before adsorption, zeolite samples were degassed under vacuum at 500°C for 6 h. The total porous volume (V_{total}) was calculated from the adsorbed volume of nitrogen at a relative pressure P/P_0 of 0.98 whereas the microporous volume (V_{micro}) was determined using the t-plot method. The mesoporous volume (V_{meso}) was obtained by the difference between V_{total} and V_{micro}.

Platinum dispersion on alumina was determined by hydrogen titration of chemisorbed oxygen (H_2–O_2 titration) in a Gira Xisorb apparatus with a thermal conductivity detector. The samples were first calcined under air at 530°C for 2 h at 5°C min^{-1}, then cooled down to room temperature and purged with He. The first reduction with H_2 was done at 450°C for 2 h with a flow of 20 NmL min^{-1}. After cooling down to room temperature and purging with He, 15 pulses with pressures from 0.5 to 60 kPa of oxygen were added until saturation occurred (oxygen titration). Another He purge was done before a second reduction with H_2 at room temperature.

Then 10 pulses with pressures from 0.5 to 60 kPa of hydrogen were added until saturation (hydrogen titration). The number of platinum surface sites was calculated based on the platinum dispersion and the total amount of platinum measured by XRF.

2.4 Catalytic tests

Ethylcyclohexane (ECH) hydroconversion tests were performed in a high-throughput catalytic test unit with sixteen fixed-bed downflow reactors. This test was performed at a total pressure of 11 bar absolute. The hydrogen to ethylcyclohexane molar ratio was set to 30, and the weight hourly space velocity (WHSV) was set to 2 grams of ethylcyclohexane per gram of catalyst per hour. The conversion was changed by changing the temperature in the 200-330°C range. For each temperature two gas chromatography (GC) analyses were performed in order to check the catalyst stability. Return points confirmed that catalyst deactivation was negligible during the test. ECH conversion, product selectivities, and turnover frequencies per acid site were calculated according to reference 33. Catalytic tests demonstrated that the chosen amount of platinum was sufficient to properly balance the zeolite.[78]

2.5 Diffusion measurements

Temporal Analysis of Products (TAP) experiments were carried out to estimate the characteristic diffusion time of ethyl-cyclohexane inside H-EU-1 and H-ZSM-50 zeolites.[59] 6 mg of the zeolite sample (200 – 300 μm) was placed between two layers of quartz particles (200 – 300 μm). A thermocouple was placed inside the reactor close to the zeolite layer. The sample was heated to 400°C (10°C/min) under vacuum and kept for 30 minutes to desorb all water. Pulse experiments were then carried out between 150 - 250°C. At the end of the temperature

cycle an experiment at 175°C was repeated to check if the sample had not changed. A mixture of 50% ethyl-cyclohexane and 50% Ar was used and the m/e of 55 and 40 were monitored. Single pulse experiments were performed with 10 pulses averaged to improve the signal over noise ratio. Data acquisition times amounted to 20 seconds with pulses rates of 0.04 Hz. Before the experiments the Knudsen regime was verified by changing the pulse intensity and normalizing the Ar data. The pulse size was below 5 nmol per pulse. Details on the modeling procedure of the data can be found in the SI section.

3. RESULTS AND DISCUSSION

3.1. The adsorbed cycloalkene species: π-complex *versus* carbenium *versus* alkoxide species

A systematic DFT study of the stability of adsorbed cycloalkenes involved in the reaction network was performed at the T10O12 site, located at the intersection between 12 MR pockets and the 10 MR channel of EUO framework structure (Figure 4). The carbenium species (including some chair and boat conformations) depicted in Figure 1 were considered, as well as the corresponding π-complexes. Some of the optimized structures are depicted in Figure 5. In all attempts to stabilize alkoxides, the optimization failed and provided the corresponding π-complexes. Considering that we were performing static calculations, this conclusion differs strongly from previous investigations performed at similar level of theory for non-cyclic alkoxide species.[43-44] This suggests that the rigidity of the cycle with respect to mobile alkyl chains is a factor that hinders species that are the closest to the framework (such as alkoxides). Performing a detailed AIMD analysis of the reaction network was beyond the scope of the present work, in particular due to the significant size of the cell and number of atoms (nearly 200 per cell). Even though, we can anticipate that the stabilization of the carbenium species with

respect to alkoxides will even be enhanced by a refined approach, as this was shown for non-cyclic species.[49-50]

Some secondary carbocations were as well analyzed and the results showed either a worse stability compared to the tertiary carbocations or the direct transformation into a tertiary carbocation by hydride shift during the geometry optimization.

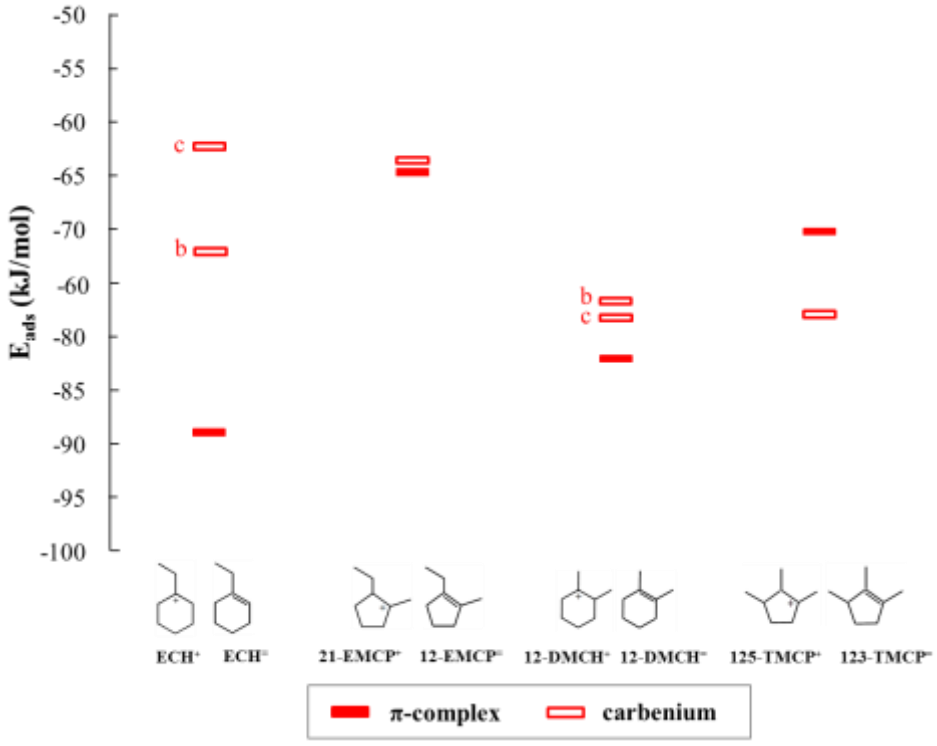

Figure 4. Adsorption energies for π-complexes and carbenium for the C_8 species considered in the present work, at the T10O12 intersection Brønsted acid site. For C_6 cycles, two conformations were considered: the chair conformation is noted "c" whereas a distorted boat one is noted "b".

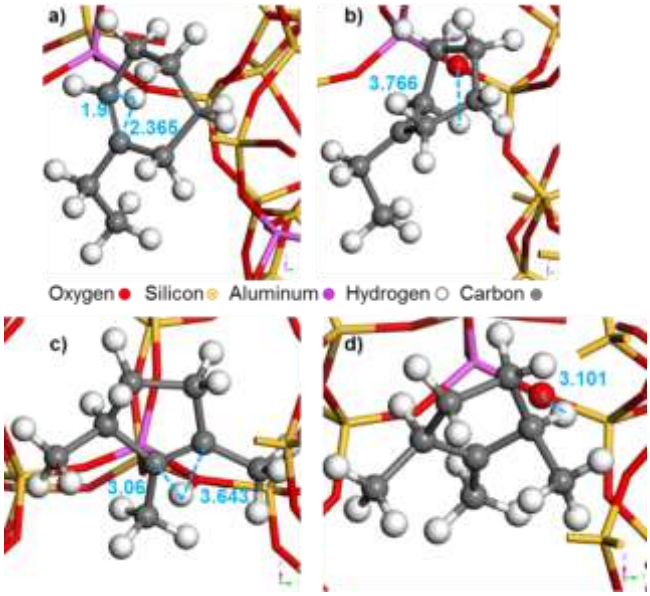

Figure 5. Structures of selected species at the T10O12 site, at the intersection between the channel and the side pocket: a) $ECH^{=}$ π -complex; b) ECH^{+} carbenium; c) 123-$TMCP^{=}$ π-complex; d) 125-$TMCP^{+}$ carbenium. For π-complexes, the distance (Å) between the proton and the carbons belonging to the double bond is given. For carbenium ions, the distance (Å) between the hydrogen which left the zeolite and the corresponding oxygen is given.

The energy of the carbenium species did not vary much as compared with the one of π-complexes. In the case of the ECH skeleton, the π-complexes are at least 25 kJ/mol more stable than the carbenium ions regardless the conformation. For the carbenium, two configurations were investigated due to their relevance in further isomerization reactions (see later): chairs and distorted boats. The chair conformation is 10 kJ/mol more stable than the distorted boat conformation. 12-EMCP and 12-DMCH related carbenium and π-complexes are very close in energy. In the case of 12-$DMCH^{+}$ chair and boat conformation energies were almost the same. Finally, for 123-TMCP, the π-complex is about 10 kJ/mol less stable than the carbenium.

In order to explain such relative energy differences, we performed structural analysis. The stability of the four π-complexes is directly correlated to the distance between the molecule and the zeolite framework: the closer to the framework, the more stable the π-complexes. The latter

was quantified by the average distance between the framework proton and the carbons belonging to the C=C double bond (Figure 6 and Table S2). The ECH π -complex was more stable than the corresponding carbocation and also closer to the zeolite. For bulkier structures, such 123-TMCP, the π-complex is slighter higher in energy compared to the corresponding carbenium. The three methyl groups of this molecule are likely at the origin of a steric constraint to approach the framework.

However, such a correlation between stability and distance was not valid for carbenium species. For these species, the O…H distance (O from the framework were the H originates, H transferred to the molecule) is reported in Figure 6. Some correlations between the energy and other distances (Al-C, C being the carbon atoms of the PCP) were also looked at but failed. Some other correlations with the local electrostatic field were also looked at, but did not reveal clear trends, contrary to previous findings for smaller hydrocarbons.[43] This suggests that the stability of these charged bulky species is a combination of several factors (likely electrostatics, van der Waals interaction, etc.) making simple descriptors irrelevant for the prediction of the nature of the most stable species at a given site in the zeolite.

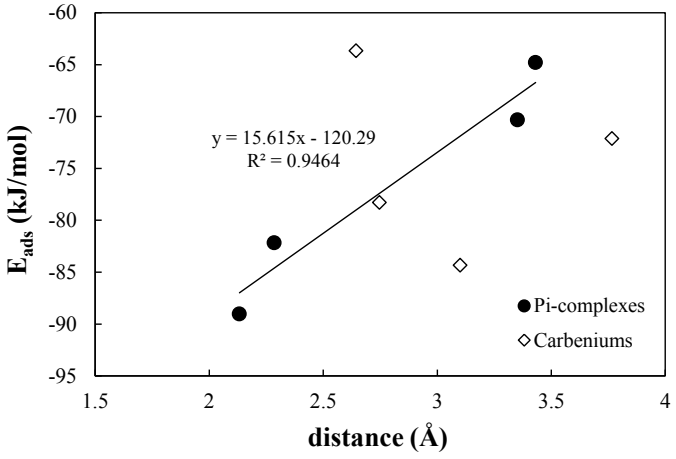

Figure 6. Correlation between adsorption energy and distance between pi-complex / carbenium ions and the zeolite framework at the intersection channel-pocket site (T10O12).

3.2. Isomerization pathway at the T10O12 intersection site

At the T10O12 intersection site between the channel and the pocket, a full study of the ethylcyclohexene isomerization pathway including proton transfer, hydride transfer and cycle contraction-expansions (Figure 1) has been performed. Starting from 1-ethylcyclohexene (ECH=) the different isomers families considered were the ethylmethylcyclopentenium (EMCP+), dimethylcyclohexenium (DMCH+) and trimethylcyclopentenium (TMCP+). They were obtained via type B isomerization, expected to take place via PCP species.

A first proton transfer from the zeolite framework to the $ECH^{=}$ π-complex is needed in order to start the isomerization reaction. This elementary step (via ts1) exhibits an energy barrier (Figure 7) around 15 kJ/mol and leads to a carbenium with a distorted chair conformation. A conformational change from a chair to a boat ECH^{+} has been found as necessary before any cycle contraction step. The energetic barrier corresponding to this conformational change (via ts2) is around 22 kJ/mol (Figure 7).

Then, the cycle contraction from ECH^{+} to the 12-$EMCP^{+}$ happens through a PCP (TS1), by a bond formation between carbons 1 and 2. The latter was obtained as a transition state, being an edge protonated cyclopropyl species (Figure 7 and Figure 8 a), with an energy barrier of 57 kJ/mol. In the course of the isomerization, the proton from carbon 2 moved to carbon 3 while the C1-C3 bond was broken. The skeleton of the transition state resembles that of the ring contraction-expansion intermediates in MTO,[54-58] with a three carbon cycle connected by an edge to a five carbon cycle. However, due to different saturation levels (number of H atoms connected to each C atom on the rings), the spatial arrangement is very different as well as the charge delocalization.

Hydride transfer from the methyl to the ethyl of the 12-EMCP$^+$ is then required in order to start the next cycle contraction (via ts3). The energetic barrier of this step was found at around 12 kJ/mol. ts1, ts2 and ts3 structures are depicted in Figure S3. Then, it appears that the cycle contraction step is by far the most energy demanding step, as compared to proton and hydride transfers, and cycle conformation change. Thus for the following steps, transition states for cycle contractions and expansions only were looked at.

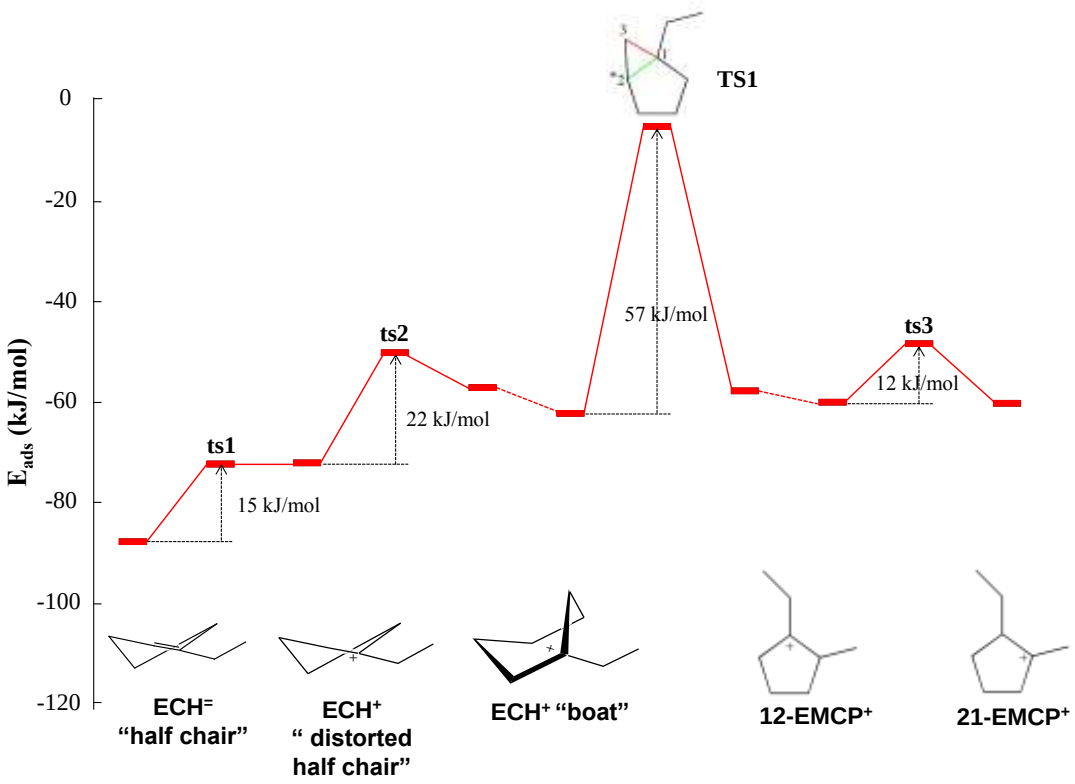

Figure 7. Energy profile at the T10O12 intersection site for the proton transfer, conformational change, first cycle contraction and hydride transfer reactions. Full lines represent the different intermediates with their corresponding TS whereas the dashed lines connect the same intermediates coming from different TS, i.e. obtained by two different IRCs. * Hydrogen shifting. The bond to be broken (in the forward direction) is depicted in red and the forming bond in green.

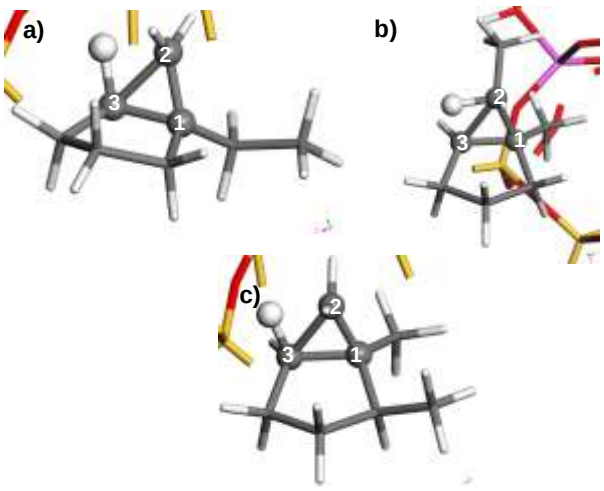

Figure 8. Different transition states at the intersection active site T10O12 a) TS1, b) TS2 and c) TS3. The carbons numbered are the ones corresponding to the PCP and the white ball corresponds to the Hydrogen atom shifting between the reactant and the product. Same color code as Figure 5.

Figure 9 (red curve for the T10O12 site) depicts the energy barriers associated to the PCP transition states, corresponding to the different cycle contraction-expansion reactions. Each transition structure was connected to a reactant and a product from the IRC. Two consecutive TS should have in common a species that is at the same time the product of the first step and the reactant of the next one. Due to small conformation changes, the energies of the two identical species obtained from the two IRCs may differ somehow, as depicted in two cases in Figure 7. In this case, we have reported the intermediate with the lowest adsorption energy hereafter.

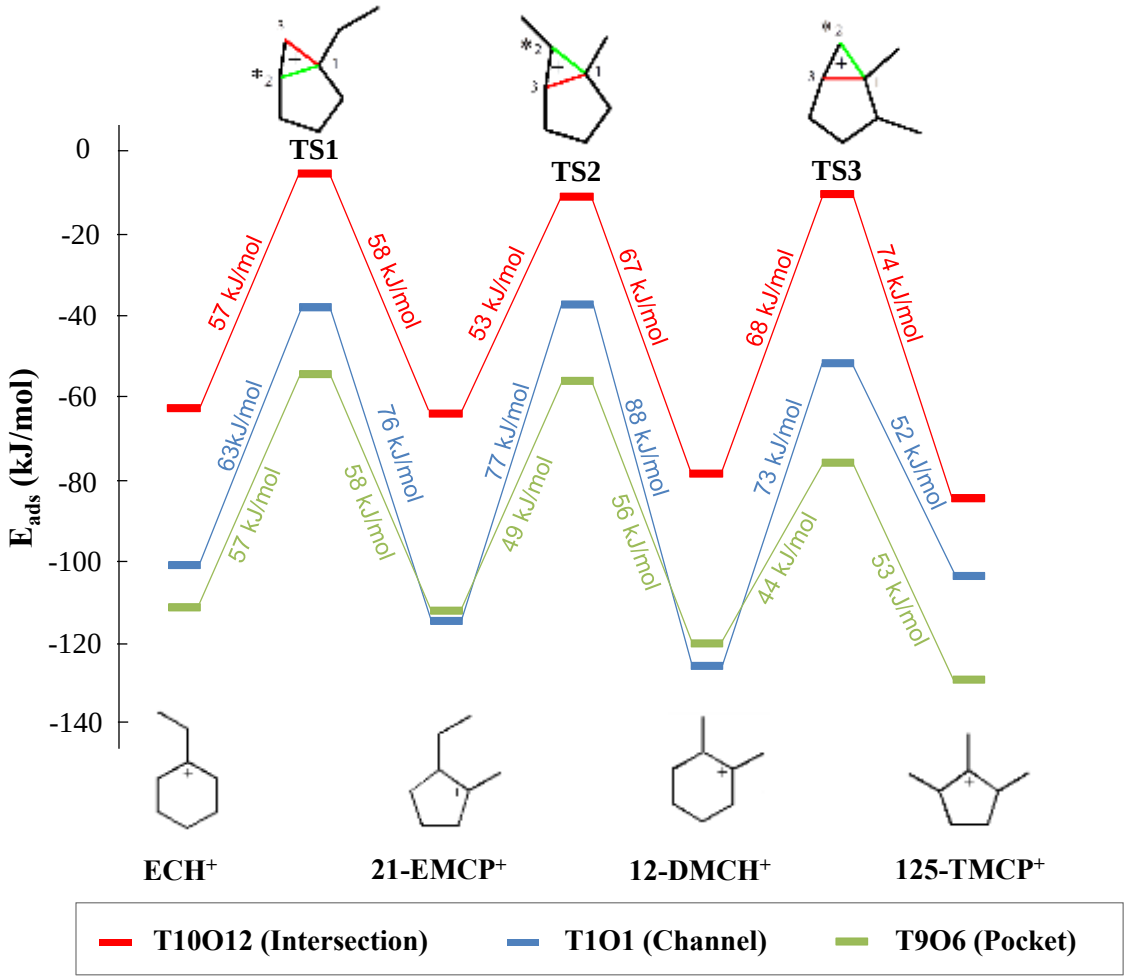

Figure 9. Energy profile for the cycle contraction-expansions through PCPs, at three sites of the EUO framework located at the 10 MR channel, the 12 MR pocket, and at their intersection. * Hydrogen shifting. The bond to be broken (in the forward direction) is depicted in red and the forming bond in green.

At this intersection site, the expansion from 21-EMCP$^+$ to 12-DMCH$^+$ exhibits a 53 kJ/mol energy barrier, very similar to the contraction barrier from ECH$^+$ to 21-EMCP$^+$ (57 kJ/mol). The following contraction from 12-DMCH$^+$ to 125-TMCP$^+$ exhibits a barrier around 68 kJ /mol. All transition structures consisted in a cyclopentane with a PCP connected edge-to-edge with the cyclopentane, and containing one of the branches in one of their vertices. The distances between the atoms in the PCP exhibited close values for all the transition states (Table 2). TS2 is slightly

different since the distance between C_2-H and C_3-H were inversed compared to the other transition states (see terminology in Figure 8). These similarities in distance, supports the close adsorption energies found for all of them, i.e. independently of the contraction or expansion of the cycle. The TS are so close that the different energy barriers are determined mainly by the energy differences of the intermediates and not by the TS themselves. Moreover, the transition states are not early nor late transition states.

Table 2. Distances between atoms in the PCP for all optimized transition structures for contraction-expansion steps, at the T10O12 intersection active site. The imaginary frequencies for the transition structures are also given (one single imaginary frequency per transition structure).

	Distance (Å)					
	C_1-C_2	C_2-C_3	C_1-C_3	C_2-H	C_3-H	f (i cm^{-1})
TS1	1.470	1.737	1.559	1.449	1.217	386
TS2	1.557	1.806	1.479	1.208	1.453	419
TS3	1.476	1.741	1.551	1.415	1.225	451

Demuth et al.[45] studied the 2-pentene isomerization in H-ZSM-22 with GGA/PW91 approximation by periodic calculations. Their most likely mechanism goes through an edge-protonated dimethylcyclopentane transition state (PCP type) similar to our TS. The energy barrier reported is 100 kJ/mol, higher than ours. Similarly, Huang et al.[46] report a barrier of 94 kJ mol^{-1} for hex-3-oxide isomerization into 3-methylpent-2-oxide, also higher than ours. The difference is not unexpected as the reactant and products are considered as alkoxides in both studies, whereas in our case, carbenium ions are intermediates.

3.3. Comparison between the different active sites within the EUO framework

First, an analysis of the stability of TS2 and of the reactants (21-EMCP$^+$) and products (12-DMCH$^+$) connected to it, has been performed over all the possible active sites of the EUO type zeolite (Figure 3). This TS had the particularity that a methyl group was linked to the carbon of the PCP edge that was not a part of the five-member ring. Figure 10 shows the energy profiles obtained for this reaction step. We failed in optimizing the transition state for two sites at the channel, T5 and T6, likely due to the difficulty of the protonated molecule to get close to the deprotonated active site, located in a poorly accessible area.

We first discuss the behavior of the sites located in the 12MR pocket. Significant differences in energy were found from one site to another, despite the structural similarities for the transition state in terms of C-C and C-H bond lengths (supporting information S4). Nevertheless, the position of this TS in the pocket differs from one active site to another (Figure S7). The energy difference could be due to the different accommodation of the TS inside the pocket, i.e. if the PCP is oriented towards the exit of the pocket (channel) or to the bottom of the pocket and if the methyl- bonded to the edge-carbon is oriented or not towards the active site. The species at T3 and T9 have similar low energies and their positions inside the pocket provided a similar local geometry for the accommodation of the TS. The PCP is oriented towards the channel and the methyl -bonded to the edge- carbon oriented in the opposite site of the active site (towards the channel). This is not the case of the other active sites.

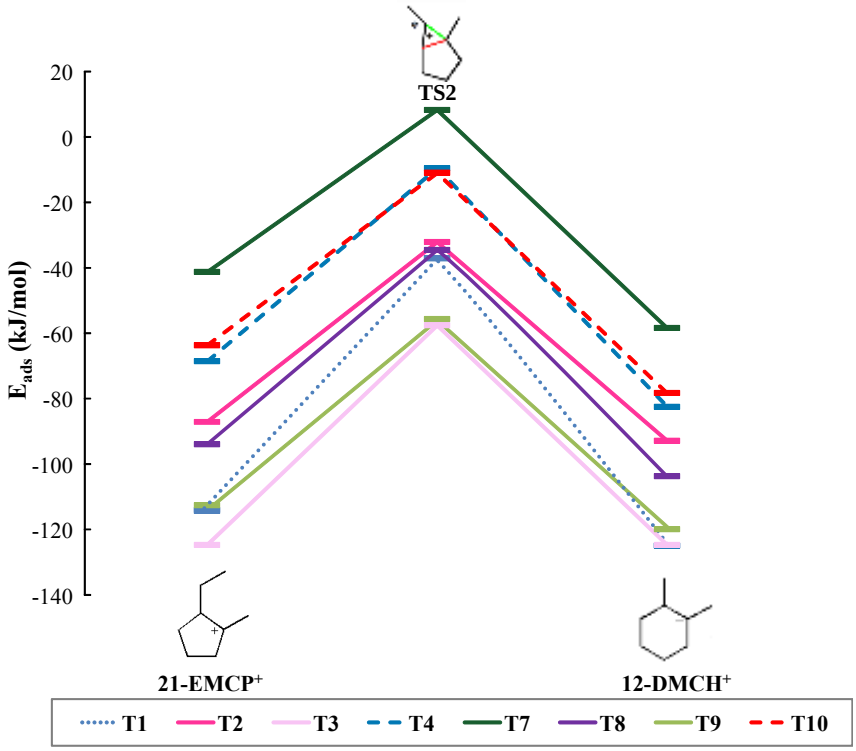

Figure 10. Energy profile for the expansions through the TS2 PCP at all the sites of the EUO type zeolite represented in Figure 3. Pocket sites: full lines, intersection sites: dashed lines, channel sites: dot lines. * Hydrogen shifting. The bond to be broken (in the forward direction) is depicted in red and the forming bond in green.

Regarding the sites located at the intersection, species located at T4 and T10 exhibited close energies, in line with their similar position at the intersection. The distance from the PCP to the active site position is, however, different in both sites as illustrated in Table S6, which seems to have no influence in the adsorption energy of the TS.

The T1 site was found as the single site able to stabilize the PCP in the channel, as explained previously. Comparing the stability of TS2 and the related reactants and products, the pocket exhibits the most stabilizing sites (T3 and T9), followed by the channel (T1), whereas the intersection (T4 and T10) had less favorable interaction with the cationic species. Some other sites of the pocket (such as T7) did not stabilize much the intermediates. Comparing the barriers from one site to the other, they are rather close (varying from 50 to 77 kJ/mol forward and from

61 to 88 kJ/mol backward, table S7). Thus, in most cases the main differences between the different actives sites are the absolute energies of the intermediates and transition states, and not so much the energy barriers of this step. This reflects a strong site-dependent confinement effect, which does not strongly depends on the nature of the carbenium species (reactant, PCP transition state, product) for a given step.

Table 3 reports the dispersion contribution to the adsorption energy for the reactant, transition state and product of this reaction step. This contribution appears to be strongly negative in all cases, but much more at the pocket and channel sites (from -134 to -101 kJ/mol) than at the intersection sites (from -84 to -59 kJ/mol). However, the dispersion term does only slightly vary along the reaction pathway, which means that the strong energy differences between transition states and intermediates are held by non-dispersive term, due to the PCP nature of the TS.

Table 3. Dispersion contribution to the adsorption energy of the 21-EMCP$^+$, TS2 and 12-DMCH$^+$ species. Note that the no transition state was identified at the T5 and T6 sites.

Site		**E_{ads}(disp) (kJ/mol)**		
Al siting	**zone**	**21-EMCP$^+$**	**TS2**	**12-DMCH$^+$**
T1	Channel	-127	-124	-121
T2	Pocket	-113	-105	-105
T3	Pocket	-119	-112	-118
T4	Intersection	-59	-59	-61
T7	Pocket	-127	-106	-134
T8	Pocket	-101	-112	-121
T9	Pocket	-117	-111	-112
T10	Intersection	-75	-77	-84

Thus, the respective behaviors of the intersection versus the channel and pocket sites are well rendered by the dispersion interaction. For the molecules considered, these disfavor the intersection site with respect to the two other kinds of sites. This is in agreement with the notion of confinement effect, which variation according to the local topology is often considered to be

of van der Waals origin,[79] and with previous computational work addressing the comparison of the stabilization of various hydrocarbons in various zeolites.[80,81-82]

We extended the comparison of various active sites to the whole reaction pathway, taking into account only the cycle contractions and expansions, and selecting one favorable site per location: one in the channel (T1O1), one in the pocket (T9O6), one at the intersection (T10O12, already investigated in section 3.2). The energy profiles are reported in Figure 9. They confirmed the much higher stability of species at the pocket and the channel as compared to the intersection, regardless the reaction intermediates and the transition states. A slight difference in terms of energy for intermediates (2-11 kJ/mol) is observed between the channel and the pocket sites, except the 125-$TMCP^+$ which was clearly more stable in the pocket than in the channel (25 kJ/mol). All transition states are lower in energy in the pocket than in the channel (16-24 kJ/mol). Similar as for TS2, the dispersion contribution to the adsorption energy was extracted for the three sites along the whole reaction pathway (Table 4). The same features are revealed, suggesting that the dispersion interactions are favoring the pocket and channel sites versus the intersection site. Note, however, that along a given pathway at a given site, the dispersion contribution is not sufficient to anticipate the stability of the ionic species considered, as shown in section 3.1. This is in agreement with previous findings devoted to the investigation of various non-cyclic carbocations. [42-44,51,80-83]

Table 4. Dispersion contribution (kJ/mol) to the adsorption energy of all the species considered in the pathway, for selected sites at the intersection, channel and pocket zone in EUO.

Species	Site		
	T10O12 Intersection	**T1O1 Channel**	**T9O6 Pocket**
ECH^+	-66	-113	-136
TS1	-61	-118	-141
21-$EMCP^+$	-75	-127	-117
TS2	-77	-124	-111
12-$DMCH^+$	-84	-121	-112
TS3	-73	-127	-149
125-$TMCP^+$	-76	-121	-150

These observations generalize our findings made before in the case of TS2 tested at all the active sites, even if the step corresponding to TS2 is not the rate-determining one for all sites. Indeed, it appears that the main differences between the three investigated acid sites is not the precise respective energy of TS1, TS2 or TS3, but the absolute energy levels of all the species (close to 50 kJ/mol in difference between the pocket and the intersection site). The origin of this is found to be the dispersion interaction term between the intermediates/transition states and the zeolite. Moreover, the maximal forward barriers are slightly lower for the pocket (57 kJ/mol) as compared to the other sites (73 kJ/mol in the channel and 68 kJ/mol at the intersection).

All these results suggests that the most probable active site for carrying out the reaction is the one located in the pocket. Thanks to an optimal confinement effect, this site stabilizes all intermediates and transition states, affecting only slightly the barriers of each elementary step. An impact on the macroscopic kinetic feature is thus expected on apparent activation energies, but mainly due to adsorption terms. Note also that we can retrospectively consider that the protonation barriers (such as the one investigated in section 3.2.) will not be very different from one site to another, and will thus stay negligible with respect to the contraction-expansion barriers.

3.4. Gibbs free energy profiles

The Gibbs free energy profiles at 277 °C, calculated according to the methods exposed in section 2 and Supporting Information S3, are depicted in Figure 11, for the T10O12, T9O6 and T1O1 sites. This temperature was chosen as it is a central temperature in the present experimental investigation (see later, section 3.4).

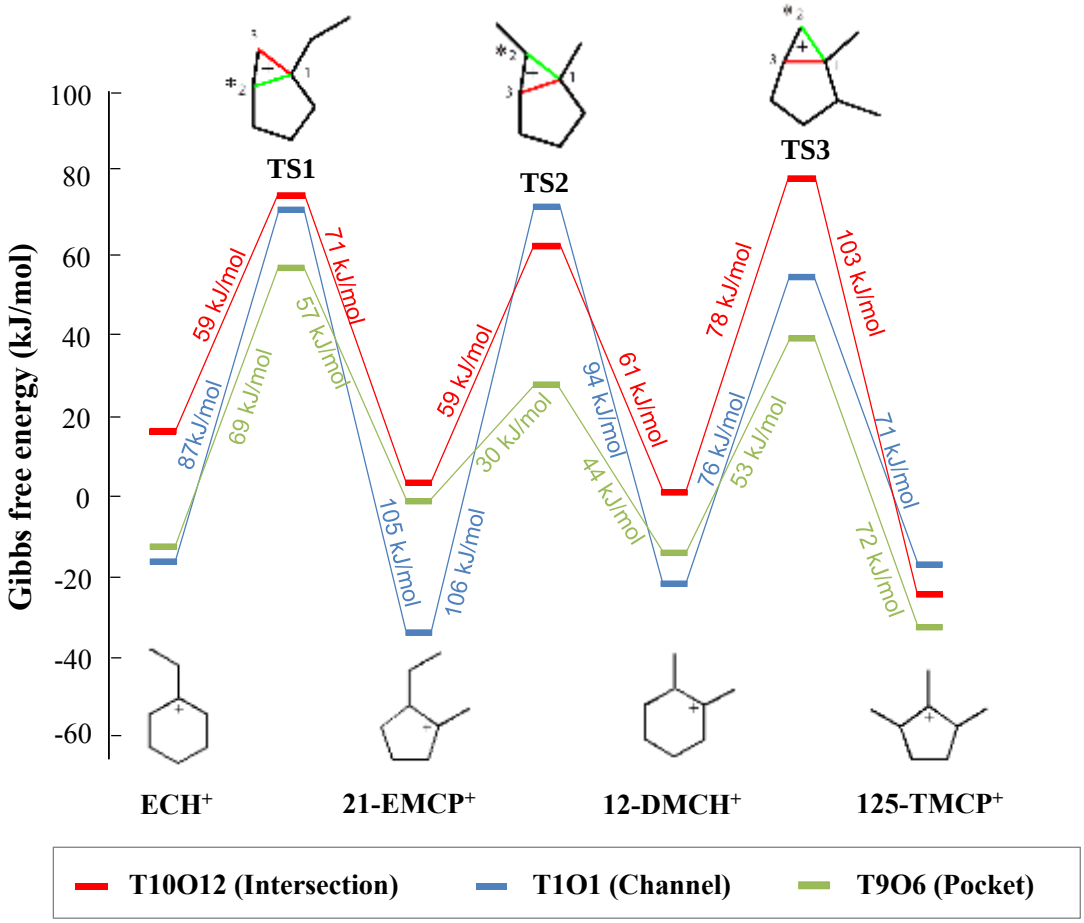

Figure 11. Adsorption Gibbs free energy profiles at the pocket (green), the channel (blue) and the intersection (red) at 277°C. * Hydrogen shifting. The bond to be broken (in the forward direction) is depicted in red and the forming bond in green.

Whereas most adsorption energies are negative (Figure 10), entropy contributions lead to positive values of free energies for transition structures, as well as for some of the intermediates.

The shape of the profiles is also affected: the Gibbs free energy profile reveals again the pocket as the most favorable site whereas the channel exhibits much higher Gibbs free energy barriers. The intersection remains a noncompetitive site with respect to the pocket and channel sites. Table S7 includes all the Gibbs energies for all the intermediates and TS. Table S8 gives all the activation data estimated from the DFT calculations.

In the case of the free energy profile at the pocket site, the intrinsic free energy barrier to pass from $ECH^{=}$ to TS1 is 69 kJ/mol (Figure 11). In the case of the intersection site, this barrier is 59 kJ/mol. Thus, the intrinsic activation free energy difference between the two sites is expected to be close to 10 kJ/mol, for the consumption of the reactant. We may also consider the apparent activation free energies for the first step, given by the difference between the activation free energy and the adsorption free energy (thus the absolute free energy of the transition state in Figure 11). At the pocket site, the apparent activation free energy is close to 56 kJ/mol, while at the intersection it is 74 kJ/mol. The difference is then 18 kJ/mol. These values will be discussed latter in comparison with experimental data (section 3.5).

3.5. Experimental characterization and catalytic evaluation of the H-EU-1 and H-ZSM-50 zeolites

XRD characterization confirmed that both solids are well crystallized and corresponded to EU-1 and ZSM-50 respectively (Supporting Information S6). The physicochemical properties of the zeolites in the protonic form are provided Table 5. The very low amount of Na compared to the framework Al (less than 4% molar) demonstrates the efficiency of the ammonium exchange. For both zeolites, the percentage of extraframework aluminum was the same, 9%, according to ^{27}Al NMR. The total amount of Brønsted acid sites per gram is 1.4 time higher for the H-EU-1

zeolite. This is a consequence of the lower Si/Al molar ratio of H-EU-1 compared to H-ZSM-50. The microporous volumes are comparable. However, the external surface area and the mesoporous volume of the H-EU-1 are substantially higher compared to H-ZSM-50. The high H-EU-1 external surface area and the significant mesoporous volume are induced by the agglomeration of round nano-crystals (30-60 nm) as revealed by SEM analysis (Supporting Information S6). Such phenomenon was reported for other zeolites such as Beta[84] or IZM-2.[85] H-ZSM-50 particles are much bigger rods (several nm of length and 200 nm of thickness).

Table 5. Physicochemical properties of the H-EU-1 and H-ZSM-50 zeolites

Sample	S_{BET} ($m^2\ g^{-1}$)	S_{ext} ($m^2\ g^{-1}$)	V_{micro} ($mL\ g^{-1}$)	V_{mes} ($mL\ g^{-1}$)	$(Si/Al)_g$ (mol/mol)	Na/Al^{IV} (%)	Al^{IV}	n_{A*} (μmol/g)
H-EU-1	438	75	0.14	0.19	18	0.3%	91%	735
H-ZSM-50	356	28	0.13	0.05	29	3.9%	91%	529

* micromoles of Brønsted acid sites per gram of zeolite

Figure 12 represents the evolution of the ECH conversion as a function of the temperature for both the bifunctional catalysts with H-ZSM-50 or H-EU-1 zeolites (table 1). The H-EU-1 bifunctional catalyst is significantly more active than the H-ZSM-50 bifunctional catalyst on a weight basis. Comparable level of ECH conversions could be obtained for temperature typically 70°C lower with H-EU-1 bifunctional catalyst. The different amount of Brønsted acid sites per gram for the two zeolites cannot account for such difference. For instance at 270°C the turnover frequency per Brønsted acid site equals 0.03 s^{-1} for H-EU-1 and 0.002 s^{-1} for H-ZSM-50. Thus the acid sites in H-EU-1 are on average, fifteen times more active than those in H-ZSM-50. Applying the Eyring's equation,[86] one can deduce the link between the ratio of TOFs

$\frac{TOF_{H-EU-1}}{TOF_{H-ZSM-50}}$ and the difference in apparent activation free energy between the two materials $\Delta_r G^{\neq^\circ}_{H-EU-1} - \Delta_r G^{\neq^\circ}_{H-ZSM-50}$ (eq.1).

$$\frac{TOF_{H-EU-1}}{TOF_{H-ZSM-50}} = e^{-\frac{\Delta_r G^{\neq^\circ}_{H-EU-1} - \Delta_r G^{\neq^\circ}_{H-ZSM-50}}{RT}} \quad \text{Eq.1}$$

This represents a difference in apparent activation free energy of $\Delta_r G^{\neq^\circ}_{H-EU-1} - \Delta_r G^{\neq^\circ}_{H-ZSM-50} = -12$ kJ/mol.

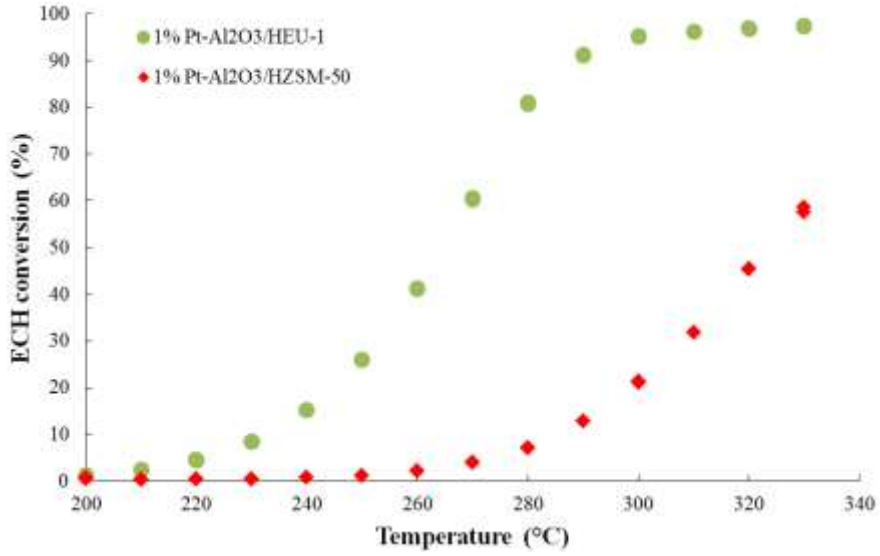

Figure 12. Ethylcyclohexane conversion versus temperature for the H-EU-1 and for the H-ZSM-50 bifunctional catalysts.

At this stage, the higher turnover frequency per acid site observed for H-EU-1 compared to H-ZSM-50 could be explained either by the different location of the active sites for the two zeolites and/or by increased diffusional limitations for H-ZSM-50 induced by its bigger crystallites sizes. Indeed, diffusion limitations were assigned an important role in the hydroconversion of n-heptane in H-EU-1.[87]

In order to evaluate the existence of possible diffusional limitations, TAP experiments were carried out. Figure S1-S2 compares the experimental and model normalized TAP pulse responses for ethyl-cyclohexane over H-ZSM-50 and H-EU-1 as a function of temperature. An adequate description of the experimental data was obtained by the model. Table S10 lists the parameter estimates from the TAP data. Rather similar adsorption enthalpies were found for both zeolite samples, as expected for zeolites with similar structures. The characteristic diffusion times are, on the other hand, different for the two zeolites. The diffusion of ethyl-cyclohexane inside the micropores of H-ZSM-50 is faster than for H-EU-1 at 175°C. However, when the values are extrapolated to the reaction temperatures applied in this study, the characteristic diffusion times become similar for both zeolites, due to the difference in activation energy for micropore diffusion. The difference in catalytic performance between the two zeolites can thus not be attributed to transport phenomena.

Thus, the location of the active site remains to explain the difference in performance between the two zeolites. It is known from literature that the active sites of the EU-1 are located in the channel and in the pocket whereas in the ZSM-50 are located in the intersection.[18-19] Thus, in full consistence with our ab initio calculations, the zeolite possessing active sites in the channel and in the pocket (H-EU-1) is much more active than the zeolite possessing active sites in the intersection (H-ZSM-50). The free energy difference of -12 kJ/mol between the two zeolites, given by the ratio of turnover frequencies (eq. 1), is in excellent agreement with the computational estimation of -10 kJ/mol, according to the difference in intrinsic activation free energy for the first step of the reaction (section 3.4). Considering apparent activation free energies (section 3.4), the difference was estimated at -18 kJ/mol, also close to the experimental value of 12 kJ/mol. This makes our conclusions based on DFT calculations even stronger,

regarding the difference in activity of both samples, as a tracer of the difference in confinement effect between the side pockets and the channel. Note that the uncertainty of DFT calculations may be higher than 10 kJ/mol, making the estimation of difference in computed activation free energy approximate. However, the fact that the order of magnitude is the same makes us confident in the validity of the conclusion.

Hence, this work suggests that DFT calculations of such reaction pathways is a relevant method for determining the location of the active sites. It also provides new insights in the mechanism of cyclic alkene transformations by Brønsted acid catalysts, which was never investigated at the atomic scale in the past.

CONCLUSIONS

In the present contribution, the location of the most active sites (for ethylcyclohexene isomerization, within the ethylcyclohexane hydroconversion bi-functional framework) within a given zeolitic framework (EUO) is elucidated by DFT calculations, and confirmed experimentally by the experimental catalytic evaluation of two zeolites (H-EU-1 and H-ZSM-50) depicting this framework but with different positions of the Brønsted acid sites. The active sites in the H-EU-1 zeolite are mainly found inside 12 MR side-pockets and in 10 MR channels, whereas in the H-ZSM-50 zeolite they are located at the intersection between the channel and the side-pocket. The DFT evaluation of the stability of intermediates and transition states revealed the intersection between the channel and the pocket as the most unfavorable active site for the reaction. On the contrary the side pocket is found as the preferred place for the reaction to happen. The origin of the differences were found to be mainly the dispersion interactions between the intermediates/transition states and the zeolite. These results were as well confirmed

by the calculation of the Gibbs adsorption energy profile. Consistently, in the experimental hydroconversion of ethylcyclohexane H-EU-1 shows a turnover frequency at 270°C fifteen times higher than H-ZSM-50. This difference in turnover frequency could be attributed either to diffusional limitations or to the active site location. However, TAP experiments revealed that the difference in catalytic performance between the two zeolites cannot be attributed to transport phenomena. Hence, the difference of activity can be attributed to the different active sites location. The experimental difference in activation free energy for the two solids very nicely match the value computed by DFT.

This study also provides detailed computational information about the reaction network for the bi-functional isomerization of naphthenes. The transition structures are PCP-like, the cyclopropane being connected edge-to-edge to a cyclopentane unit. A typical feature of the transition states is the presence of an edge proton, migrating along the cycle contraction-expansion step. This work opens the door to the computational design of zeolitic catalysts from ab initio investigations.

ASSOCIATED CONTENT

AUTHOR INFORMATION

Corresponding Author

*Email: celine.chizallet@ifpen.fr

Notes

The authors declare no competing financial interest.

Supporting Information.

Additional figures and tables, regarding DFT procedures, equations and results are given in the Supporting Information file as well as some characterization data from experiments. Additional information as noted in the text. This information is available free of charge via the Internet at http://pubs.acs.org.

ACKNOWLEDGMENT

The authors acknowledge Tomáš Bučko for providing line minimizations and intrinsic reaction coordinate algorithms, and Pascal Raybaud (IFP Energies nouvelles) for fruitful discussions. This work was performed using HPC resources from GENCI-IDRIS (Grant 2016-x20160816) and the IFPEN ENER110 supercomputer. Christophe James and Véronique Delattre (IFP Energies nouvelles) are acknowledged for their assistance in performing the catalytic testing experiments.

REFERENCES

(1) Vermeiren, W.; Gilson, J. P., Impact of Zeolites on the Petroleum and Petrochemical Industry, *Topics Catal.* **2009**, *52*, 1131-1161.

(2) Deka, U.; Lezcano-Gonzalez, I.; Weckhuysen, B. M.; Beale, A. M., Local Environment and Nature of Cu Active Sites in Zeolite-Based Catalysts for the Selective Catalytic Reduction of NOx, *ACS Catal.* **2013**, *3*, 413-427.

(3) Jacobs, P. A.; Dusselier, M.; Sels, B. F., Will Zeolite-Based Catalysis be as Relevant in Future Biorefineries as in Crude Oil Refineries?, *Angew. Chem. Int. Ed.* **2014**, *53*, 8621-8626.

(4) Ennaert, T.; Van Aelst, J.; Dijkmans, J.; De Clercq, R.; Schutyser, W.; Dusselier, M.; Verboekend, D.; Sels, B. F., Potential and Challenges of Zeolite Chemistry in the Catalytic Conversion of Biomass, *Chem. Soc. Rev.* **2016**, *45*, 584-611.

(5) Li, C.; Vidal-Moya, A.; Miguel, P. J.; Dedecek, J.; Boronat, M.; Corma, A., Selective Introduction of Acid Sites in Different Confined Positions in ZSM-5 and Its Catalytic Implications, *ACS Catal.* **2018**, *8*, 7688-7697.

(6) Gallego, E. M.; Portilla, M. T.; Paris, C.; León-Escamilla, A.; Boronat, M.; Moliner, M.; Corma, A., "Ab initio" Synthesis of Zeolites for Preestablished Catalytic Reactions, *Science* **2017**, *355*, 1051–1054.

(7) Yarulina, I.; De Wispelaere, K.; Bailleul, S.; Goetze, J.; Radersma, M.; Abou-Hamad, E.; Vollmer, I.; Goesten, M.; Mezari, B.; Hensen, E. J. M.; Martínez-Espín, J. S.; Morten, M.; Mitchell, S.; Perez-Ramirez, J.; Olsbye, U.; Weckhuysen, B. M.; Van Speybroeck, V.; Kapteijn, F.; Gascon, J., Structure–Performance Descriptors and the Role of Lewis Acidity in the Methanol-to-Propylene Process, *Nature Chem.* **2018**, *10*, 804-812.

(8) Knott, B. C.; Nimlos, C. T.; Robichaud, D. J.; Nimlos, M. R.; Kim, S.; Gounder, R., Consideration of the Aluminum Distribution in Zeolites in Theoretical and Experimental Catalysis Research, *ACS Catal.* **2017**, *8*, 770-784.

(9) Pinar, A. B.; Verel, R.; Pérez-Pariente, J.; van Bokhoven, J. A., Direct Evidence of the Effect of Synthesis Conditions on Aluminum Siting in Zeolite Ferrierite: A ^{27}Al MQ MAS NMR Study, *Microporous Mesoporous Mater.* **2014**, *193*, 111-114.

(10) van Bokhoven, J. A.; Koningsberger, D. C.; Kunkeler, P.; van Bekkum, H.; Kentgens, A. P. M., Stepwise Dealumination of Zeolite Beta at Specific T-Sites Observed with ^{27}Al MAS and ^{27}Al MQ MAS NMR, *J. Am. Chem. Soc.* **2000**, *122*, 12842-12847.

(11) Vjunov, A.; Fulton, J. L.; Huthwelker, T.; Pin, S.; Mei, D.; Schenter, G. K.; Govind, N.; Camaioni, D. M.; Hu, J. Z.; Lercher, J. A., Quantitatively Probing the Al Distribution in Zeolites, *J. Am. Chem. Soc.* **2014**, *136*, 8296-8306.

(12) Brus, J.; Kobera, L.; Schoefberger, W.; Urbanova, M.; Klein, P.; Sazama, P.; Tabor, E.; Sklenak, S.; Fishchuk, A. V.; Dedecek, J., Structure of Framework Aluminum Lewis sites and Perturbed Aluminum atoms in Zeolites as Determined by ^{27}Al{^{1}H} REDOR (3Q) MAS NMR Spectroscopy and DFT/Molecular Mechanics, *Angew. Chem. Int. Ed.* **2015**, *54*, 541-545.

(13) Sklenak, S.; Dedecek, J.; Li, C.; Wichterlova, B.; Gabova, V.; Sierka, M.; Sauer, J., Aluminum Siting in Silicon-Rich Zeolite Frameworks: A Combined High-Resolution ^{27}Al NMR Spectroscopy and Quantum Mechanics/Molecular Mechanics Study of ZSM-5, *Angew. Chem., Int. Ed* **2007**, *46*, 7286-7289.

(14) Holzinger, J.; Beato, P.; Lundegaard, L. F.; Skibsted, J., Distribution of Aluminum over the Tetrahedral Sites in ZSM-5 Zeolites and Their Evolution after Steam Treatment, *J. Phys. Chem. C* **2018**, *122*, 15595-15613.
(15) Perea, D. E.; Arslan, I.; Liu, J.; Ristanovic, Z.; Kovarik, L.; Arey, B. W.; Lercher, J. A.; Bare, S. R.; Weckhuysen, B. M., Determining the Location and Nearest Neighbours of Aluminium in Zeolites with Atom Probe Tomography, *Nature Commun.* **2015**, *6*, 7589.
(16) van Bokhoven, J. A.; Lee, T. L.; Drakopoulos, M.; Lamberti, C.; Thieβ, S.; Zegenhagen, J., Determining the Aluminium Occupancy on the Active T-Sites in Zeolites using X-Ray Standing Waves, *Nat. Mater.* **2008**, *7*, 551-555.
(17) Agostini, G.; Lamberti, C.; Palin, L.; Milanesio, M.; Danilina, N.; Xu, B.; Janousch, M.; van Bokhoven, J. A., In Situ XAS and XRPD Parametric Rietveld Refinement To Understand Dealumination of Y Zeolite Catalyst, *J. Am. Chem. Soc.* **2010**, *132*, 667-678.
(18) Souverijns, W.; Rombouts, L.; Martens, J. A.; Jacobs, P. A., Molecular Shape Selectivity of EUO Zeolites, *Micropor. Mater.* **1995**, *4*, 123-130.
(19) Peral, I.; Jones, C. Y.; Varkey, S. P.; Lobo, R. F., Structural Comparison of Two EUO-Type Zeolites Investigated by Neutron Diffraction, *Microporous Mesoporous Mater.* **2004**, *71*, 125-133.
(20) Moreau, F.; Moreau, P.; Gnep, N. S.; Magnoux, P.; Lacombe, S.; Guisnet, M., Ethylbenzene Isomerization over Bifunctional Platinum Alumina–EUO Catalysts: Location of the Active Sites, *Microporous Mesoporous Mater.* **2006**, *90*, 327-338.
(21) Marcilly, C. *Acido-Basic Catalysis*; Technip: Paris, 2005.
(22) Cannella, W. J.,Xylenes and Ethylbenzene, In *Kirk-Othmer Encyclopedia of Chemical Technology*; John Wiley & Sons, I., Ed. 2007.
(23) Guisnet, M., "Ideal" Bifunctional Catalysis over Pt-Acid Zeolites, *Catal. Today* **2013**, *218-219*, 123-134.
(24) Weitkamp, J.; Ernst, S.; Karge, H. G., Peculiarities in the Conversion of Naphthenes on Bifunctional Catalysts, *Erdoel Kohle, Erdgas, Petrochem.* **1984**, *37*, 457–462.
(25) Weitkamp, J.; Jacobs, P. A.; Ernst, S.,Shape Selective Isomerization and Hydrocracking of Naphthenes Over Pt/HZSM-5 Zeolite, In *Stud. Surf. Sci. Catal.*; Jacobs, P. A., Jaeger, N. I., Jírů, P., Kazansky, V. B., Schulz-Ekloff, G., Eds.; Elsevier: 1984; Vol. 18, p 279-290.
(26) Weitkamp, J.; Ernst, S.,Comparison Of The Reactions Of Ethylcyclohexane And 2-Methylheptane On Pd/Lay Zeolite, In *Stud. Surf. Sci. Catal.*; Imelik, B., Naccache, C., Coudurier, G., Taarit, Y. B., Vedrine, J. C., Eds.; Elsevier: 1985; Vol. 20, p 419-426.
(27) Mihindou-Koumba, P. C.; Cerqueira, H. S.; Magnoux, P.; Guisnet, M., Methylcyclohexane Transformation over HFAU, HBEA, and HMFI Zeolites: II. Deactivation and Coke Formation, *Ind. Eng. Chem. Res.* **2001**, *40*, 1042-1051.
(28) Martens, G. G.; Thybaut, J. W.; Marin, G. B., Single-Event Rate Parameters for the Hydrocracking of Cycloalkanes on Pt/US-Y Zeolites, *Ind. Eng. Chem. Res.* **2001**, *40*, 1832-1844.
(29) McVicker, G. B.; Feeley, O. C.; Ziemiak, J. J.; Vaughan, D. E. W.; Strohmaier, K. C.; Kliewer, W. R.; Leta, D. P., Methylcyclohexane Ring-Contraction: A Sensitive Solid Acidity and Shape Selectivity Probe Reaction, *J. Phys. Chem. B* **2005**, *109*, 2222-2226.
(30) Weitkamp, J., Catalytic Hydrocracking—Mechanisms and Versatility of the Process, *ChemCatChem* **2012**, *4*, 292-306.

(31) Ribeiro, F.; Marcilly, C.; Guisnet, M., Hydroisomerization of n-Hexane on Platinum Zeolites: I. Kinetic Study of the Reaction on Platinum/Y-Zeolite Catalysts: Influence of the Platinum Content, *J. Catal.* **1982**, *78*, 267-274.
(32) F., C.; M., G.; R., M., Tracer Study of the Isomerization of Paraffins on Bifunctional Catalysts, *Proceedings of the Sixth International Congress on Catalysis* **1977**, *1*, 478-487.
(33) Gutierrez-Acebo, E.; Leroux, C.; Chizallet, C.; Schuurman, Y.; Bouchy, C., Metal/Acid Bifunctional Catalysis and Intimacy Criterion for Ethylcyclohexane Hydroconversion: When Proximity Does Not Matter, *ACS Catal.* **2018**, *8*, 6035-6046.
(34) Ivanova, I. I.; Kolyagin, Y. G., Impact of in Situ MAS NMR Techniques to the Understanding of the Mechanisms of Zeolite Catalyzed Reactions, *Chem. Soc. Rev.* **2010**, *39*, 5018-5050.
(35) Denayer, J. F.; Baron, G. V.; Vanbutsele, G.; Jacobs, P. A.; Martens, J. A., Evidence for Alkylcarbenium Ion Reaction Intermediates from Intrinsic Reaction Kinetics of C6–C9 n-Alkane Hydroisomerization and Hydrocracking on Pt/H–Y and Pt/USY Zeolites, *J. Catal.* **2000**, *190*, 469-473.
(36) Thybaut, J.; Narasimhan, C. S. L.; Marin, G.; Denayer, J. M.; Baron, G.; Jacobs, P.; Martens, J., Alkylcarbenium Ion Concentrations in Zeolite Pores During Octane Hydrocracking on Pt/H-USY Zeolite, *Catal. Lett.* **2004**, *94*, 81-88.
(37) Kazansky, V. B., Adsorbed Carbocations as Transition States in Heterogeneous Acid Catalyzed Transformations of Hydrocarbons, *Catal. Today* **1999**, *51*, 419-434.
(38) Rigby, A. M.; Frash, M. V., Ab Initio Calculations on the Mechanisms of Hydrocarbon Conversion in Zeolites: Skeletal Isomerisation and Olefin Chemisorption, *J. Mol. Catal. A* **1997**, *126*, 61-72.
(39) Rigby, A. M.; Kramer, G. J.; van Santen, R. A., Mechanisms of Hydrocarbon Conversion in Zeolites: A Quantum Mechanical Study, *J. Catal.* **1997**, *170*, 1-10.
(40) Boronat, M.; Corma, A., Are Carbenium and Carbonium Ions Reaction Intermediates in Zeolite-Catalyzed Reactions?, *Appl. Catal. A* **2008**, *336*, 2-10.
(41) Boronat, M.; Viruela, P. M.; Corma, A., Reaction Intermediates in Acid Catalysis by Zeolites: Prediction of the Relative Tendency To Form Alkoxides or Carbocations as a Function of Hydrocarbon Nature and Active Site Structure, *J. Am. Chem. Soc.* **2004**, *126*, 3300-3309.
(42) Rozanska, X.; van Santen, R. A.; Demuth, T.; Hutschka, F.; Hafner, J., A Periodic DFT Study of Isobutene Chemisorption in Proton-Exchanged Zeolites: Dependence of Reactivity on the Zeolite Framework Structure, *J. Phys. Chem. B* **2003**, *107*, 1309-1315.
(43) Leydier, F.; Chizallet, C.; Costa, D.; Raybaud, P., Revisiting Carbenium Chemistry on Amorphous Silica-Alumina: Unraveling their Milder Acidity as Compared to Zeolites, *J. Catal.* **2015**, *325*, 35-47.
(44) Rey, J.; Raybaud, P.; Chizallet, C., Ab Initio Simulation of the Acid Sites at the External Surface of Zeolite Beta, *ChemCatChem* **2017**, *9*, 2176-2185.
(45) Demuth, T.; Rozanska, X.; Benco, L.; Hafner, J.; van Santen, R.; Toulhoat, H., Catalytic Isomerization of 2-Pentene in H-ZSM-22—A DFT Investigation, *J. Catal.* **2003**, *214*, 68-77.
(46) Huang, B.; Bai, P.; Neurock, M.; Davis, R. J., Conversion of n-Hexane and n-Dodecane over H-ZSM-5, H-Y and Al-MCM-41 at Supercritical Conditions, *Appl. Catal. A* **2017**, *546*, 149-158.

(47) Tuma, C.; Kerber, T.; Sauer, J., The tert-Butyl Cation in H-Zeolites: Deprotonation to Isobutene and Conversion into Surface Alkoxides, *Angew. Chem. Int. Ed.* **2010**, *49*, 4678-4680.
(48) Tuma, C.; Sauer, J., Protonated Isobutene in Zeolites: tert-Butyl Cation or Alkoxide?, *Angew. Chem. Int. Ed.* **2005**, *44*, 4769-4771.
(49) Hajek, J.; Van der Mynsbrugge, J.; De Wispelaere, K.; Cnudde, P.; Vanduyfhuys, L.; Waroquier, M.; Van Speybroeck, V., On the Stability and Nature of Adsorbed Pentene in Brønsted Acid Zeolite H-ZSM-5 at 323K, *J. Catal.* **2016**, *340*, 227-235.
(50) Cnudde, P.; De Wispelaere, K.; Van der Mynsbrugge, J.; Waroquier, M.; Van Speybroeck, V., Effect of Temperature and Branching on the Nature and Stability of Alkene Cracking Intermediates in H-ZSM-5, *J. Catal.* **2017**, *345*, 53-69.
(51) Vollmer, J. M.; Truong, T. N., Mechanisms of Hydrogen Exchange of Methane with H-Zeolite Y: An ab Initio Embedded Cluster Study, *J. Phys. Chem. B* **2000**, *104*, 6308-6312.
(52) Yang, S.; Kondo, J. N.; Domen, K., Formation of Alkenyl Carbenium ions by Adsorption of Cyclic Precursors on Zeolites, *Catal. Today* **2002**, *73*, 113-125.
(53) Cuán, A.; Martínez-Magadán, J. M.; García-Cruz, I.; Galván, M., DFT—Quantum Chemical Study of the HZSM-5-Cyclohexene Interaction Pathways, *J. Mol. Catal. A* **2005**, *236*, 194-205.
(54) McCann, D. M.; Lesthaeghe, D.; Kletnieks, P. W.; Guenther, D. R.; Hayman, M. J.; Van Speybroeck, V.; Waroquier, M.; Haw, J. F., AComplete Catalytic Cycle for Supramolecular Methanol-to-Olefins Conversion by Linking Theory with Experiment, *Angew. Chem., Int. Ed.* **2008**, *47*, 5179.
(55) Van Speybroeck, V.; De Wispelaere, K.; Van der Mynsbrugge, J.; Vandichel, M.; Hemelsoet, K.; Waroquier, M., First principle chemical kinetics in zeolites: the methanol-to-olefin process as a case study, *Chem. Soc. Rev.* **2014**, *43*, 7326-7357.
(56) Wang, C.-M.; Wang, Y.-D.; Liu, H.-X.; Xie, Z.-K.; Liu, Z.-P., Theoretical Insight into the Minor Role of Paring Mechanism in the Methanol-to-Olefins Conversion within HSAPO-34 Catalyst, *Microporous Mesoporous Mater.* **2012**, *158*, 264-271.
(57) Sun, Y.; Zheng, D.; Pei, S.; Fan, D., New Theoretical Insights into the Contributions of Poly(methylbenzene) and Alkene Cycles to the Methanol to Propene Process in H-FAU Zeolite, *J. Phys. Chem. C* **2017**, *121*, 16216-16237.
(58) Wang, S.; Chen, Y.; Wei, Z.; Qin, Z.; Ma, H.; Dong, M.; Li, J.; Fan, W.; Wang, J., Polymethylbenzene or Alkene Cycle? Theoretical Study on Their Contribution to the Process of Methanol to Olefins over H-ZSM-5 Zeolite, *J. Phys. Chem. C* **2015**, *119*, 28482-28498.
(59) Gleaves, J. T.; Yablonskii, G. S.; Phanawadee, P.; Schuurman, Y., TAP-2: An Interrogative Kinetics Approach, *Appl. Catal. A* **1997**, *160*, 55-88.
(60) Perdew, J.; Burke, K.; Ernzerhof, M., Generalized Gradient Approximation Made Simple, *Phys. Rev. Lett.* **1996**, *77*, 3865-3868.
(61) Kresse, G.; Hafner, J., Ab Initio Molecular-Dynamics Simulation of the Liquid-Metal-Amorphous-Semiconductor Transition in Germanium, *Phys. Rev. B* **1994**, *49*, 14251-14269.
(62) Kresse, G.; Furthmüller, J., Efficiency of Ab-Initio Total Energy Calculations for Metals and Semiconductors using a Plane-Wave Basis Set, *Comput. Mat. Sci.* **1996**, *6*, 15-50.
(63) Kresse, G.; Joubert, D., From Ultrasoft Pseudopotentials to the Projector Augmented-Wave Method, *Phys. Rev. B* **1999**, *59*, 1758-1775.

(64) Grimme, S., Semiempirical GGA-Type Density Functional Constructed with a Long-Range Dispersion Correction, *J. Comput. Chem.* **2006**, *27*, 1787-1799.
(65) Baerlocher, C.; McCusker, J. K., *Database of Zeolite Structures:* http://www.iza-structure.org/databases/.
(66) Guillon, E.; Lacombe, S.; Sozinho, T.; Magnoux, P.; Gnep, S.; Moreau, P.; Guisnet, M., How to Improve the Selectivity of Zeolitic Catalysts in C_8 Aromatic Cut Isomerization, *Oil & Gas Science and Technology - Revue de l'IFP* **2009**, *64*, 731-744.
(67) Martins, J.; Birot, E.; Guillon, E.; Lemos, F.; Ramôa Ribeiro, F.; Magnoux, P.; Laforge, S., Sodium Exchange over H-EU-1 Zeolite. Part I: Physicochemical Characterization, *Microporous Mesoporous Mater.* **2013**, *171*, 230-237.
(68) Bucko, T.; Benco, L.; Demuth, T.; Hafner, J., Ab Initio Density Functional Investigation of the (001) Surface of Mordenite, *J. Chem. Phys.* **2002**, *117*, 7295-7305.
(69) Demuth, T.; Hafner, J.; Benco, L.; Toulhoat, H., Structural and Acidic Properties of Mordenite. An ab Initio Density-Functional Study, *J. Phys. Chem. B* **2000**, *104*, 4593-4607.
(70) Henkelman, G.; Jonsson, H., Improved Tangent Estimate in the Nudged Elastic Band Method for Finding Minimum Energy Paths and Saddle Points, *J. Chem. Phys.* **2000**, *113*, 9978-9985.
(71) Fleurat-Lessard, P.; Dayal, P., http://pfleurat.free.fr/ReactionPath.php, *Accessed April 2nd 2016*.
(72) Pulay, P., Convergence Acceleration of Iterative Sequences. The Case of SCf Iteration, *Chem. Phys. Lett.* **1980**, *73*, 393-398.
(73) Henkelman, G.; Jónsson, H., A Dimer Method for Finding Saddle Points on High Dimensional Potential Surfaces using only First Derivatives, *J. Chem. Phys.* **1999**, *111*, 7010-7022.
(74) Heyden, A.; Bell, A. T.; Keil, F. J., Efficient Methods for Finding Transition States in Chemical Reactions: Comparison of Improved Dimer Method and Partitioned Rational Function Optimization Method, *J. Chem. Phys.* **2005**, *123*, 224101.
(75) Bučko, T.; Benco, L.; Hafner, J.; Ángyán, J. G., Monomolecular Cracking of Propane over Acidic Chabazite: An Ab Initio Molecular Dynamics and Transition Path Sampling Study, *J. Catal.* **2011**, *279*, 220-228.
(76) Fukui, K., The Path of Chemical Reactions - the IRC Approach, *Acc. Chem. Res.* **1981**, *14*, 363-368.
(77) Fukui, K., Formulation of the Reaction Coordinate, *J. Phys. Chem.* **1970**, *74*, 4161-4163.
(78) Weisz, P. B., Polyfunctional Heterogeneous Catalysis, *Adv. Catal.* **1962**, *13*, 137-190.
(79) Derouane, E. G., Shape Selectivity in Catalysis by Zeolites: The Nest Effect, *J. Catal.* **1986**, *100*, 541-544.
(80) Mansoor, E.; Van der Mynsbrugge, J.; Head-Gordon, M.; Bell, A. T., Impact of Long-Range Electrostatic and Dispersive Interactions on Theoretical Predictions of Adsorption and Catalysis in Zeolites, *Catal. Today* **2018**, *312*, 51-65.
(81) Fang, H.; Zheng, A.; Xu, J.; Li, S.; Chu, Y.; Chen, L.; Deng, F., Theoretical Investigation of the Effects of the Zeolite Framework on the Stability of Carbenium Ions, *J. Phys. Chem. C* **2011**, *115*, 7429-7439.
(82) Song, B.; Chu, Y.; Li, G.; Wang, J.; Lo, A.-Y.; Zheng, A.; Deng, F., Origin of Zeolite Confinement Revisited by Energy Decomposition Analysis, *J. Phys. Chem. C* **2016**, *120*, 27349-27363.

(83) De Moor, B. A.; Reyniers, M.-F. o.; Sierka, M.; Sauer, J.; Marin, G. B., Physisorption and Chemisorption of Hydrocarbons in H-FAU Using QM-Pot(MP2//B3LYP) Calculations, *J. Phys. Chem. C* **2008**, *112*, 11796-11812.
(84) Coutanceau, C.; Da Silva, J. M.; Alvarez, M. F.; Ribeiro, F. R.; Guisnet, M., Dealumination of Zeolites. Part VII. Influence of the Acid Treatment of a HBEA Zeolite on the Framework Composition and on the Porosity, *J. Chim. Phys.* **1997**, *94*, 765-781.
(85) Marques Mota, F.; Bouchy, C.; Guillon, E.; Fécant, A.; Bats, N.; Martens, J. A., IZM-2: A Promising New Zeolite for the Selective Hydroisomerization of Long-Chain n-Alkanes, *J. Catal.* **2013**, *301*, 20-29.
(86) Eyring, H., The Activated Complex in Chemical Reactions, *J. Chem. Phys.* **1935**, *3*, 107-115.
(87) Raybaud, P.; Patrigeon, A.; Toulhoat, H., The Origin of the C7-Hydroconversion Selectivities on Y, β, ZSM-22, ZSM-23, and EU-1 Zeolites, *J. Catal.* **2001**, *197*, 98-112.

GRAPHICAL TOC